2016 IEEE International Conference on Advanced Intelligent Mechatronics (AIM)
Banff, Alberta, Canada, July 12–15, 2016

Constrained Optimal Control of Needle Deflection for Semi-Manual Steering

Carlos Rossa, Mohsen Khadem, Ronald Sloboda, Nawaid Usmani, and Mahdi Tavakoli

Abstract— **Brachytherapy is a widely used treatment for patients with localized cancer where high doses of radiation are administered to cancerous tissue by implanting radioactive seeds into the prostate using long beveled-tip needles. Accurate seed placement is an important factor that influences the outcome of the treatment. In this paper, we present and study the suitability of a new framework for computer-assisted needle steering during seed implantation in brachytherapy. The framework is based on a hand held brachytherapy needle steering apparatus. As the needle is manually inserted, the device automatically rotates the needle's base axially at appropriate depths inside tissue in order to control the trajectory of the needle tip towards a target. The steering controller is based on the Rapidly Exploring Random Tree algorithm that updates the necessary manoeuvres online. Experimental results performed in phantom and ex-vivo biological tissues show an average absolute targeting error of 0.56 $\pm$0.62 and 0.48 $\pm$0.48 mm, respectively.**

I. Introduction

Prostate cancer is the most frequently diagnosed cancer in males worldwide, with 1.1 million estimated cases in 2012 [1]. Because of the ageing population, the number of diagnosed prostate cancers is expected to significantly increase in the near future. For instance, in Canada, the projected number of cases is expected to dramatically rise from 24,000 in 2015 to 42,000 by 2032 [2].

Transperineal permanent prostate brachytherapy (PPB) is a widely used treatment option for patients with localized cancer due to its favourable toxicity profile and minimally-invasiveness. In this procedure, high doses of radiation are administered to cancerous tissue by implanting a large number of radioactive seeds into the prostate using long beveled-tip needles. The seeds are deployed to achieve a pre-operatively developed seed distribution in order to eradicate the cancer while sparing healthy adjacent structures. Therefore, accurate seed placement in predefined targets corresponding to the desired seed distribution is an important factor that influences the outcome of the treatment.

Typically, the needle is assumed to follow a straight path towards the target. In practice, however, the needle deflects from this optimal path as it cuts through and compresses the tissue. This can significantly compromise the implant quality and lead to undesirable side effects. As a result, the success of PPB strongly relies on surgeons with sufficient expertise and case volumes. Hence, making PPB more accessible for inexperienced surgeons and for those with lower case volumes is necessary in response to the growing need for this treatment.

To improve seed placement accuracy, robotics-assisted needle steering and seed implantation have been the focus of significant research over the past decade. Several needle steering devices have been developed to steer needles and deposit radioactive seed; [3], [4], [5], [6], [7] and [8] are only a few examples. These systems generally rely on the fact that, in brachytherapy, needles with an asymmetric bevel tip are used to easily penetrate and cut through tissue. As the needle is pushed through tissue, an imbalance of forces is created at the needle tip, leading the needle to deflect from an assumed straight trajectory and instead follow a curved path [9], [10], [11]. This inherent deflection can be used to steer the needle towards its target by properly changing the orientation of the bevel via axial rotation of the needle base such that the needle tip is forced to follow a path as close as possible to the assumed straight trajectory.

One can classify these systems into three main categories depending on the degree of needle steering automation, i.e., fully automated insertion, semi-automated insertion, and fully manual insertion. In the first category the needle insertion is performed automatically by a needle steering robot [5], [4]. In the second category, the robotic system acts as a needle holder that can rotate the needle axially, with the physician being responsible for needle insertion [12], [6]. Finally the third class comprises technologies designed to provide the physician with relevant information about the necessary manoeuvres and keep her/him in control of both insertion and steering procedures, such as visual and tactile feedback devices [8], [13], [14].

Each category listed above has advantages and drawbacks. In the first and second types, needle insertion manoeuvres can be precisely performed by robots brought into the operating room. On the other hand, this may require significant adaptation of the brachytherapy procedure which can limit clinical acceptance. In the third category, only additional information is provided to the physician. Hence, he/she must be able to precisely perform the required steering manoeuvres, which still depends heavily on the physician's experience and skills.

In this paper, we propose a novel framework for assisted

This work was supported by the Natural Sciences and Engineering Research Council (NSERC) of Canada under grant CHRP 446520, the Canadian Institutes of Health Research (CIHR) under grant CPG 127768, and by the Alberta Innovates - Health Solutions (AIHS) under grant CRIO 201201232.

Carlos Rossa, Mohsen Khadem, and Mahdi Tavakoli are with the Department of Electrical and Computer Engineering, University of Alberta, Edmonton, AB, Canada T6G 2V4. E-mail: rossa@ualberta.ca; mohsen.khadem@ualberta.ca; madhi.tavakoli@ualberta.ca.

Nawaid Usmani and Ron Sloboda are with the Cross Cancer Institute and the Department of Oncology, University of Alberta, Edmonton, AB, Canada T6G 1Z2. E-mail: {ron.sloboda, nawaid.usmani}@albertahealthservices.ca.

needle steering in brachytherapy that combines manual needle insertion and automated steering manoeuvres. Unlike the systems referred to above, we use a compact apparatus for needle steering designed to enhance the surgeon's ability to position the needle during manual insertion. For safety and clinical acceptance reasons, the device (shown in Fig. 1) is designed to keep the surgeon in charge of needle insertion and to not have to modify either the operating room setup or the current brachytherapy practice. A constrained optimal controller uses ultrasound images of the needle in tissue and a needle-tissue interaction model to predict future needle deflection and automatically rotate the needle axially at appropriate insertion depth, to control the needle tip trajectory, as the surgeon manually inserts it. We validate this semi-automated needle insertion framework using a Rapidly Exploring Random Tree algorithm that calculates the optimal needle rotation depths online. The proposed framework for semi-automated needle insertion into the prostate is novel. To the author's knowledge, the only similar work consists of a device for biopsy presented in [15] with extendible curved stylet, which is not designed for PPB.

The rest of the paper is organized as follows. In Section II, we briefly discuss the workings of the needle insertion assistant system and its potential application to PPB. In Section III, we implement a constrained needle steering controller based on the Rapidly Exploring Random Tree algorithm. Experimental results in phantom and ex-vivo biological tissue reported in Section IV confirm the suitability of the proposed framework for assisted needle steering with an average needle targeting accuracy of 0.52 mm over 20 needle insertions.

II. The Needle Steering Device

The proposed framework for assisted needle insertion is based on the compact needle steering device shown in Fig. 1. A complete description of the device can be found in [16]. It is made of a 3D printed handle that the surgeon holds. A standard 18-gauge brachytherapy needle, which can be loaded with radioactive seeds, is connected to the front of the device through the hollow shaft via a quick-release mechanism. While the surgeon uses the device to insert the needle, the 3D position of the apparatus is measured online by an optical motion tracker (BB2-BWHx60 from Claron Tech, Toronto, Canada). The position of the grid and the distance from the grid template to the tissue are known. Thereby, the needle insertion depth can then be determined. This design allows the stylet to be inserted in the needle shaft such that the surgeon can manipulate it in order to deploy the seeds in tissue. As in current brachytherapy practice, once the needle reaches the target, the surgeon can hold the stylet in place and withdraw the needle and the device such that the stylet pushes the seeds out of the needle shaft for deposition in the tissue.

As the surgeon manually inserts the needle, a compact actuation unit (see Fig. 1(b)) rotates the needle axially at appropriate rotation depths such that the needle tip follows a desired trajectory towards its target. To allow for precise and

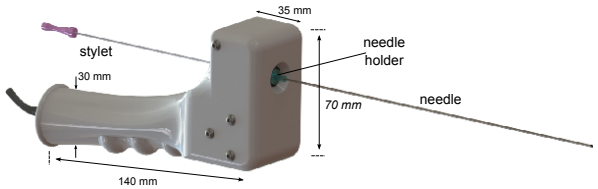

(a) CAD of the needle insertion assistant

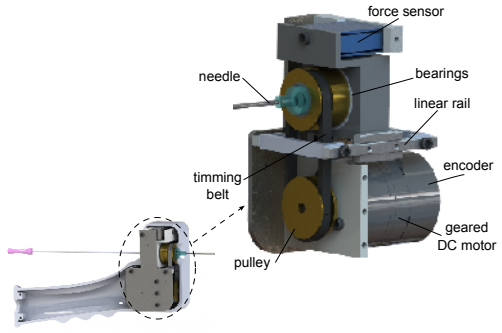

(b) Compact actuation unit for needle rotation

Fig. 1. The proposed surgeon assistant for assisted manual needle steering. The device *automatically* rotates a standard brachytherapy needle as the user *manually* inserts it in tissue. A force sensor connected the linear rail structure shown in (b) (not used in this paper) can measure the insertion force online.

fast rotation of the needle base, the actuation unit comprises a miniature motor (model 26195024SR from Faulhaber, Croglio, Switzerland) that is connected to the needle via a pulley and belt mechanism. The motor has a reduction ratio of 33:1 and an incremental encoder with 16 pulses per revolution that measures the angular position of the needle with 0.17 degree accuracy. The motor is powered by a pulse-width modulation (PMW) drive and a proportional?integral?derivative (PID) controller that calculates the required PWM duty cycle in order to control the angular position of the needle shaft. The maximal rotation velocity is 200 degrees per second.

The whole device weighs 160 grams, making it easy to incorporate with current insertion techniques and is designed not to change either the current brachytherapy procedure or the operating room settings. Although the device is designed to reduce the surgeon's workload, it still allows the surgeon to perform manual needle steering manoeuvres such as applying lateral forces to the needle shaft to affect its deflection towards the target, increasing/decreasing the insertion speed, etc. Needle rotation is preformed automatically by a needle steering controller. In the next section, the needle steering controller is developed to work in tandem with the needle steering apparatus.

III. Constrained Steering Control

As the surgeon inserts the needle, the assistant rotates it at appropriate depths to minimize targeting error at a given depth. The algorithm used to calculate these optimal rotation depths is composed of two main steps. First, it predicts the needle deflection further along the insertion process for different rotation depth candidates. Next, the optimal rotation

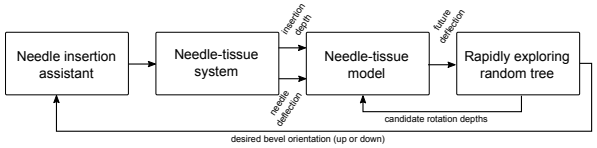

Fig. 2. Overview of needle steering controller. A needle-tissue interaction model [17] is used to estimate the needle deflection for different needle rotation depths. This information is fed into a rapidly exploring random tree algorithm that adaptively updates the rotation depths by evaluating the needle targeting accuracy.

depths is identified and updated as the insertion progresses (see Fig. 2).

In prostate brachytherapy, the target is typically defined on a straight line starting at the needle entry point in tissue and ending a certain depth. There is no need to generate 3D trajectories in such a context, thus we will limit the model here to planar needle deflections. We will employ the needle-tissue interaction model we presented in [17], which can be identified using only transverse ultrasound images of the needle in tissue, readily available clinically. The inputs to the model are the needle insertion depth, the current needle deflection, and the rotation depth(s). The model outputs the future needle tip trajectory and the needle shape.

Knowing the future needle deflections, one can evaluate the targeting accuracy and adaptively calculate the optimal rotation depths. To this end, we will use the Rapidly Exploring Random Tree (RRT) algorithm [18], [19]. RRT is an efficient sampling algorithm to quickly search high-dimensional spaces that have algebraic constraints such as the number of allowed needle rotations, by randomly building a space-filling tree. The tree is constructed incrementally from samples drawn randomly from the search space and is inherently biased to grow towards large unsearched areas of the problem. For the purpose of needle steering, the optimization algorithm interactively evaluates the effects of rotations at different depths on the needle targeting accuracy. This optimization problem needs to account for constraints on the order in which the rotations take place (second rotation must be at a higher depth than the first one) which makes the RRT useful to reduce the search space and optimize computation time.

The inputs of the RRT are the target point $\mathscr{T}$, the candidate rotation depths $\mathscr{C} \in \mathbb{R}^N$ comprised of locations between the current and the maximum depths, the number N of allowed rotations in the remaining insertion horizon, the current position of the needle shaft X_0, and the computation time available for planning Γ_{max}. First, the algorithm selects N random rotation depth candidates q_{rand} from $\mathscr{C}$ (See `Rand_Conf` in Algorithm 1.). Next, `Near_Vertex` runs through all the vertexes (candidate rotation depths) in the space $\mathscr{G}$ to find the closest vertex to q_{rand}. `New_Conf` accepts the random configuration as a new vertex as long as the rotations succeed each other with increasing depths (rotation n takes place at a higher depth than rotation $n-1$), and if all the rotation depth candidates are higher that the

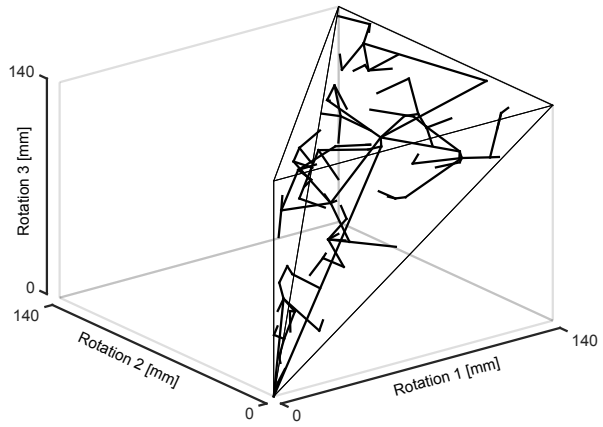

(a) RRT iterative search

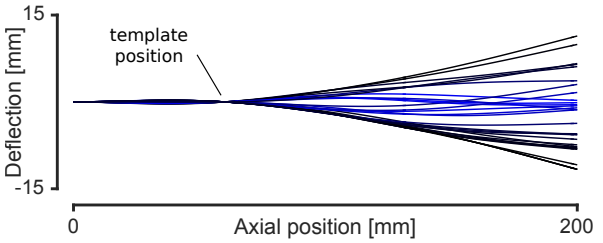

(b) Corresponding needle shaft deflection

Fig. 3. Example of the RRT interactive search for the optimal rotation depths. In (a), each axis corresponds to the depth at which the needle is rotated. In (b) the resultant needle shaft deflection for the rotation points determined in (a) for a 200 mm long brachytherapy needle inserted to a depth of 140 mm through a rigid grid template in a hypothetical tissue sample.

current insertion depth. Next, needle tip path and targeting accuracy (p_{new}) are obtained by inputting the selected rotation depths in the needle-tissue interaction model [17]. When the needle path for the newly added configuration is found to lie in the target region ($\mathscr{T}$), or when the computation times exceeds Γ_{max} the RRT planner terminates and q_{rand} contains the optimal rotation depths χ that will bring the needle towards $\mathscr{T}$.

In prostate brachytherapy, the needle insertion point and the target are typically on the same horizontal line. Throughout this paper, we assume that the target is at a depth of 140 mm. In order to limit tissue trauma, we will limit the total number of needle axial rotations to three. An example of how the RRT iterates to construct the vertices and find the optimal rotation depths is shown in Fig. 3(a). Each axis corresponds to the depth at which the needle is rotated in the search process. The constraints imposed on the candidate rotation depths reduce the full cube to the tetrahedral shown in the figure. The obtained needle targeting accuracy is evaluated for each vertex (rotation depth candidates) as shown in Fig. 3(b).

As the needle is inserted, the RRT will update the optimal needle rotation depth based on the current deflection of the needle shaft, thereby accounting for tissue heterogeneity and other factors such as tissue deformations. When the needle passes through the first optimal rotation depth, the needle is

rotated and the algorithm restarts in order to calculate the subsequent rotation depths.

Algorithm 1: $\chi \longleftarrow$ `RRT_Algorithm` $(\mathscr{C}, \mathscr{T}, N, \Gamma_{max})$

```
G ⟵ Initialize_tree (X_0)
while χ = ∅ or Γ < Γ_max do
    q_rand ⟵ Rand_Conf (C)
    q_near ⟵ Near_Vertex (q_rand, G)
    q_new ⟵ New_Conf (q_rand, q_near)
    p_new ⟵ Needle-tissue-model[17] (q_new)
    G ⟵ Add_Vertex(q_new)
    G ⟵ Add_Edge(q_new, q_near)
    if p_new ∈ T then
        χ ⟵ Extract_Conf(q_new)
    end
end
```

The RRT has been used for needle steering in [18]. Unlike the approach presented here, [18] searches all the feasible needle trajectories toward a target, as obtained from a non-holonomic model of the needle. The algorithm then solves the inverse kinematics of the model to find the rotation inputs for following the selected trajectory. In contrast, our search space is constrained by the possible control inputs directly and by the number and depths of rotations,. Therefore, there is no need to solve for inverse kinematics of the model, which makes the optimization problem faster.

IV. Experimental Setup and Results

Fig. 4(a) shows the experimental setup used to demonstrate the suitability of the proposed system. The needle is inserted using the hand-held assistant into a piece of tissue through a standard brachytherapy template grid (D0240018BK, from CR Brad, USA). The needle used in the experiments is a 200 mm long 18-gauge standard brachytherapy needle from Eckert & Ziegler Inc., USA. As the needle is inserted in the tissue, a 4DL14-5/38 linear ultrasound probe connected to a Sonix Touch ultrasound machine (Ultrasonix, Canada) slides on the tissue surface and acquires at 30 Hz transverse 2D ultrasound images of the needle. A linear stage motorized by a DC motor controls the position of the ultrasound probe, while its absolute position is measured by a linear potentiometer (LP-250FJ from Midori Precisions, Japan, not visible in Fig. 4(a)). The ultrasound imaging plane is initially placed close to the needle tip. As the needle is pushed into the tissue, the motorized linear stage controlled by a discrete PID controller moves in synchrony with the needle insertion device such that the same point close to the needle tip is always visible in the image. Each transverse ultrasound image is then processed in order to obtain the current needle tip deflection using the algorithm presented in [20]. For safety reasons, the motorised linear stage that translates the ultrasound probe is activated only when the needle is inserted through the grid template.

We perform needle insertion in two different tissue samples. The first sample (see Fig. 4(b)) is made of plastisol gel (M-F Manufacturing Co., USA) mixed with 20% of plastic softener to yield a Young's modulus of 25.5 kPa, which is similar to the elastic modulus of human glandular tissue. The second tissue (see Fig. 4(c)) is prepared by embedding a piece of pork tenderloin in industrial gelatin derived from acid-cured tissue (gel strength 300 from Sigma-Aldrich Corporation, USA). The gelatin layer is only used to create a flat surface and to ensure good acoustic contact between the ultrasound probe and the tissue. This tissue presents different layers of muscle and fat, which makes it highly non-homogeneous.

The maximum computation time allowed for planning via the RRT algorithm is set to 1 second, which was found to provide good convergence. Hence the closed loop control scheme runs at 1 Hz. The algorithm runs to always find three best depth for the three possible needle rotations in each insertion.

A. Experimental Results

In each tissue sample, the needle is inserted up to a depth of 140 mm. Fig. 5 shows the obtained needle tip deflection as a function of the needle insertion depth in both tissue samples when the steering controller is not activated (i.e., the needle is not rotated). The final needle tip deflection is about 14 mm in plastisol and 12 mm in biological tissue.

In order to minimize the needle deflection at the maximum depth, the RRT controller is activated in the subsequent insertions. The needle is inserted 10 times in each tissue sample. The obtained average needle tip deflection in shown in Fig. 5. The path followed by the needle tip in each insertion and the average depth (blue) at which the needle base is axially rotated by 180° and its standard deviation (gray) are presented in Fig. 6 (top and bottom panels, respectively). 0° indicates the needle deflects upwards and 180° indicates that the needle deflects downwards. The average rotation depths, average maximum deflection from the straight line, and the obtained targeting accuracy are summarized in Table I. The absolute average targeting error (tip deflection at the maximum depth) in the plastisol tissue is 0.56 ±0.62 mm. In the experiments performed in biological tissue, we obtained an average absolute error of 0.48 ±0.60 mm. In both cases, this corresponds to 96% less deflection compared to the insertions without deflection control.

TABLE I

Average steering results. Units are in millimetres.

	Plastisol		Biological	
	average	deviation	average	deviation
Rotation depth 1	26.8	±2.5	32.1	± 6.4
Rotation depth 2	39.9	±7.0	48.0	±14.8
Rotation depth 3	61.1	±9.7	70.7	±21.4
Max. deflection	2.34	±0.78	1.53	±0.41
Targeting error	**0.56**	±0.62	**0.48**	±0.60

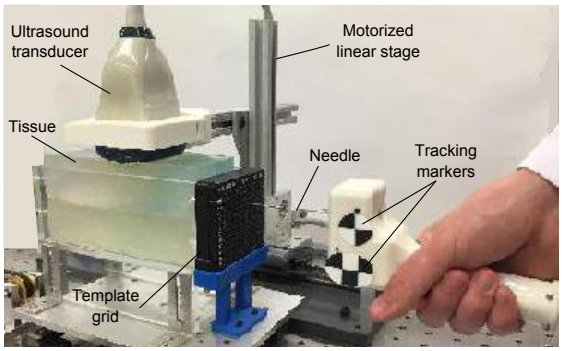

(a) Experimental setup

(b) Plastisol phantom tissue

(c) Ex-vivo biological tissue

Fig. 4. Experimental setup used for assisted brachytherapy needle steering (a). The needle is inserted into pastisol (b) and biological (c) tissue samples using the proposed assistant through a grid template. The 3D position of the device is measured using the tracking markers and an optical motion tracker (not visible). An ultrasound probe follows the tracking markers to acquire transverse images of the needle as it is inserted.

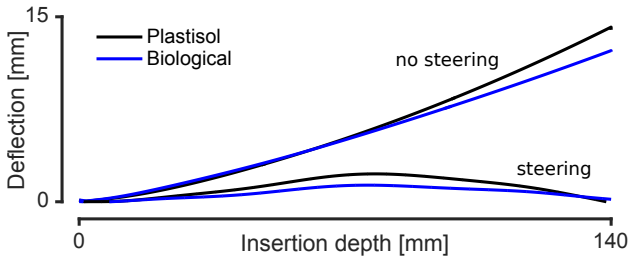

Fig. 5. Example of needle deflection without steering controller (one insertion without rotation) and average needle tip deflection with RRT steering controller over 10 insertions in each tissue sample.

B. Discussion

We have evaluated the ability of proposed system to steer a standard brachytherapy needle towards a desired target in a homogeneous (plastisol) and a heterogeneous (biological) tissue. On average, the absolute needle targeting accuracy is 0.5 mm when averaged over a total of 20 needle insertions.

The experimental results shown in Fig. 6 demonstrate that the needle can be steered towards a target following different paths. The results also indicate that the controller is responsive to tissue non-homogeneity, as it can be seen from the variability in the depths at which the needle is rotated during insertion in each tissue. The standard deviation from the average depth of rotation in the heterogeneous tissue is consistently higher compared to the homogeneous tissue. This suggests that the RRT algorithm is able to compensate for deviations of the needle from the predicted path by adjusting the rotation depths on the fly.

The needle targeting error can be partially attributed to uncertainties in the images used as ground truth due to noises present in the ultrasound images. In addition, to ensure the needle is always visible in the images, the ultrasound probe follows the needle tip but lags 3 to 5 mm behind the needle tip, which can introduce a deflection measurement error of 0.3 mm. More importantly, in the current version, the controller is designed to steer the needle in a single deflection plane. Due to heterogeneities in the tissue, and small inadvertent rotation of the needle base induced by the operator, the needle may deviate from a single plane and deflect in the 3D space, which is not accounted for in the needle-tissue interaction model used here. Another source of error can be attributed to tissue displacement induced by the ultrasound probe as it moves on the tissue surface in order to track the needle tip. In brachytherapy, this can lead to displacement of the target location and deviation of the needle from the predicted path. A solution to this limitation can be sought in using a thin, firm sleeve in which the transrectal ultrasound probe translates such that when the transducer moves, it does not deform the prostate gland and/or adjacent anatomical structures. Another option involves using an ultrasound system that can translate the imaging plane internally in a stationary probe such as the 3D2051 anorectal ultrasound probe from BK Ultrasound, USA.

Alternatively, other means of deflection measurement can also be considered, such as force sensor based estimators [21], partial ultrasound image feedback algorithms designed to minimize the ultrasound probe motion [22], or 3D ultrasound imaging [12].

V. Concluding Remarks

In this paper, we discussed a new framework for needle steering in permanent prostate brachytherapy. In contrast to existing systems, this approach relies on a hand-held needle steering apparatus and is compatible with standard brachytherapy needles. The device works with a needle steering algorithm that *automatically* rotates the needle at optimal rotation depths as the surgeon *manually* inserts it such that the needle tip reaches a desired target. Hence, the surgeon is in control of the procedure and the proposed framework does not require modifications in the operating room. The device is compact and weighs only 160 grams, making it easy to incorporate with current insertion techniques.

The proposed Rapidly Exploring Random Tree controller interactively evaluates the effects of axial needle rotations at different depths, via a needle-tissue interaction model, on the needle targeting accuracy. This is performed as the needle is inserted and the optimal rotation depths are updated as the needle insertion progresses. This optimization algorithm accounts for constraints on the order in which the rotations take place which makes the RRT useful to reduce the search space and optimize computation time.

Overall, the obtained needle target accuracy using the proposed controller is about 0.5 mm. Reducing seed placement error to this order can enable new potential applications of brachytherapy at it allows one to move away from treating the entire prostate uniformly and considering an accurate

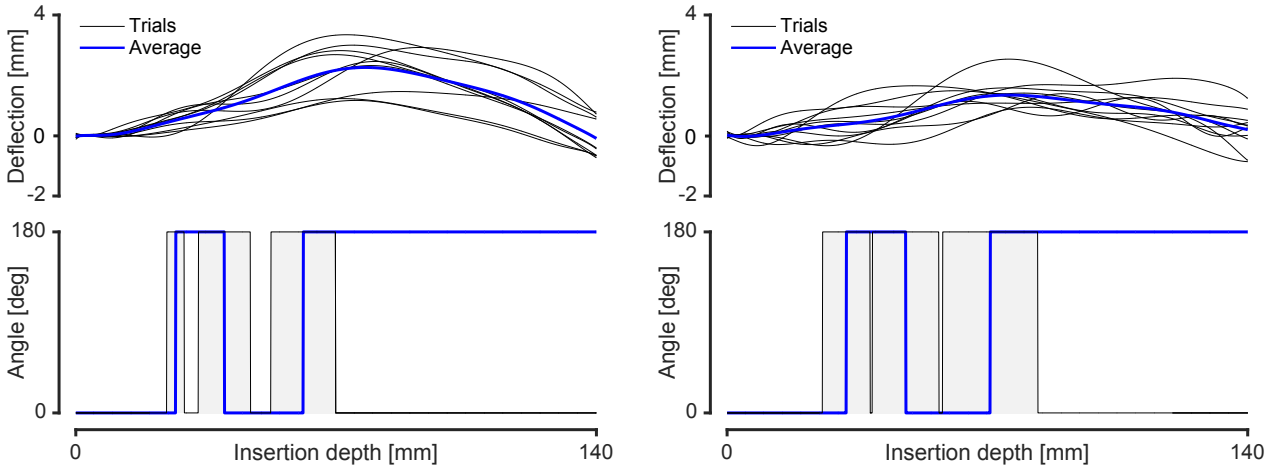

(a) Needle deflection in plastisol with RRT controller

(b) Needle deflection in biological tissue with RRT controller

Fig. 6. Experimental results with RRT controller in plastisol phantom (a) and biological tissue (b). The top panel in each sub-plot shows the needle tip deflection for each of the 10 needle insertions (gray) and the average needle tip position (blue). In the bottom panel, the average depth at which the needle is rotated (blue) and the standard deviation (gray) is shown by the change in angle of the needle base.

brachytherapy boost or focal treatment of dominant intra-prostatic lesions. Also, this technology can be considered for marker seed placement for external beam radiotherapy or targeted biopsies of suspicious lesions.

Future efforts will focus on evaluating the ability of the system to implant seeds at specific target locations while avoiding obstacles. The device's capabilities can also be extended to, in addition to guiding the needle towards the target location, automatically depositing the seeds once the target is reached, allowing one to register the position of the implanted seeds and monitor the implant's quality online.

REFERENCES

[1] L. A. Torre, F. Bray, R. L. Siegel, J. Ferlay, J. Lortet-Tieulent, and A. Jemal, "Global cancer statistics, 2012," *CA: a cancer journal for clinicians*, vol. 65, no. 2, pp. 87–108, 2015.

[2] C. Sandoval, K. Tran, R. Rahal, G. Porter, S. Fung, C. Louzado, J. Liu, H. Bryant, S. P. S. Committee, T. W. Group, *et al.*, "Treatment patterns among canadian men diagnosed with localized low-risk prostate cancer," *Current Oncology*, vol. 22, no. 6, p. 427, 2015.

[3] T. K. Podder, L. Beaulieu, B. Caldwell, R. A. Cormack, J. B. Crass, A. P. Dicker, A. Fenster, G. Fichtinger, M. A. Meltsner, M. A. Moerland, *et al.*, "AAPM and GEC-ESTRO guidelines for image-guided robotic brachytherapy: Report of task group 192," *Medical physics*, vol. 41, no. 10, p. 101501, 2014.

[4] M. Muntener et al., "Magnetic resonance imaging compatible robotic system for fully automated brachytherapy seed placement," *Urology*, vol. 68, no. 6, pp. 1313–1317, 2006.

[5] A. Patriciu, D. Petrisor, M. Muntener, D. Mazilu, M. Schar, and D. Stoianovici, "Automatic brachytherapy seed placement under mri guidance," *IEEE Transactions on Biomedical Engineering*, vol. 54, no. 8, pp. 1499–1506, Aug 2007.

[6] Y. Zhang et al., "Semi-automated needling and seed delivery device for prostate brachytherapy," in *Intelligent Robots and Systems, 2006 IEEE/RSJ International Conference on*, Oct 2006, pp. 1279–1284.

[7] N. J. Cowan, K. Goldberg, G. S. Chirikjian, G. Fichtinger, R. Alterovitz, K. B. Reed, V. Kallem, W. Park, S. Misra, and A. M. Okamura, "Robotic needle steering: Design, modeling, planning, and image guidance," in *Surgical Robotics*. Springer, 2011, pp. 557–582.

[8] C. Rossa, J. Fong, N. Usmani, R. Sloboda, and M. Tavakoli, "Multi-actuator haptic feedback on the wrist for needle steering guidance in brachytherapy," *IEEE Robotics and Automation Letters*, vol. PP, no. 99, pp. 1–1, 2016.

[9] S. Misra, K. B. Reed, B. W. Schafer, K. Ramesh, and A. M. Okamura, "Mechanics of flexible needles robotically steered through soft tissue," *The International journal of robotics research*, 2010.

[10] A. M. Okamura, C. Simone, and M. Leary, "Force modeling for needle insertion into soft tissue," *IEEE Transactions on Biomedical Engineering*, vol. 51, no. 10, pp. 1707–1716, 2004.

[11] R. Webster et al., "Nonholonomic modeling of needle steering," *The International Journal of Robotics Research*, vol. 25, no. 5-6, pp. 509–525, 2006.

[12] Z. Wei, G. Wan, L. Gardi, G. Mills, D. Downey, and A. Fenster, "Robot-assisted 3D-TRUS guided prostate brachytherapy: system integration and validation," *Medical physics*, vol. 31, no. 3, pp. 539–548, 2004.

[13] D. Magee, Y. Zhu, R. Ratnalingam, P. Gardner, and D. Kessel, "An augmented reality simulator for ultrasound guided needle placement training," *Medical & biological engineering & computing*, vol. 45, no. 10, pp. 957–967, 2007.

[14] S. Basu, J. Tsai, and A. Majewicz, "Evaluation of tactile guidance cue mappings for emergency percutaneous needle insertion," in *IEEE Haptics Symposium*, 2016.

[15] S. Okazawa, R. Ebrahimi, J. Chuang, S. E. Salcudean, and R. Rohling, "Hand-held steerable needle device," *IEEE/ASME Transactions on Mechatronics*, vol. 10, no. 3, pp. 285–296, 2005.

[16] C. Rossa, N. Usmani, R. Sloboda, and M. Tavakoli, "A hand-held assistant for semi-automated percutaneous needle steering," *IEEE Transactions on Biomedical Engineering*, p. In press, 2016.

[17] C. Rossa, M. Khadem, R. Sloboda, N. Usmani, and M. Tavakoli, "Adaptive quasi-static modelling of needle deflection during steering in soft tissue," *Robotics and Automation Letters, IEEE*, vol. PP, no. 99, pp. 1–1, 2016.

[18] S. M. LaValle and J. J. Kuffner, "Randomized kinodynamic planning," *The International Journal of Robotics Research*, vol. 20, no. 5, pp. 378–400, 2001.

[19] S. Patil et al., "Needle steering in 3D via rapid replanning," *IEEE Transactions on Robotics*, vol. 30, no. 4, pp. 853–864, 2014.

[20] M. Waine, C. Rossa, R. Sloboda, N. Usmani, and M. Tavakoli, "3D needle shape estimation in TRUS-guided prostate brachytherapy using 2D ultrasound images," *IEEE Journal of Biomedical and Health Informatics*, vol. PP, no. 99, pp. 1–1, 2015.

[21] T. Lehmann, C. Rossa, N. Usmani, R. Sloboda, and M. Tavakoli, "A virtual sensor for needle deflection estimation during soft-tissue needle insertion," in *Robotics and Automation (ICRA), 2015 IEEE International Conference on*. IEEE, 2015, pp. 1217–1222.

[22] C. Rossa, R. Sloboda, N. Usmani, and M. Tavakoli, "Estimating needle tip deflection in biological tissue from a single transverse ultrasound image: application to brachytherapy," *International journal of computer assisted radiology and surgery*, pp. 1–13, 2015.